JCI The Journal of Clinical Investigation

# Identifying and targeting pathogenic PI3K/AKT/mTOR signaling in IL-6 blockade–refractory idiopathic multicentric Castleman disease

David C. Fajgenbaum, … , Frits van Rhee, Thomas S. Uldrick

*J Clin Invest.* 2019;129(10):4451-4463. https://doi.org/10.1172/JCI126091.

Clinical Medicine | Hematology | Immunology

Idiopathic multicentric Castleman disease (iMCD) is a hematologic illness involving cytokine-induced lymphoproliferation, systemic inflammation, cytopenias, and life-threatening multi-organ dysfunction. The molecular underpinnings of interleukin-6 (IL-6) blockade–refractory patients remain unknown; no targeted therapies exist. In this study, we searched for therapeutic targets in IL-6 blockade–refractory iMCD patients with the thrombocytopenia, anasarca, fever/elevated C-reactive protein, reticulin myelofibrosis, renal dysfunction, organomegaly (TAFRO) clinical subtype.

We analyzed tissues and blood samples from 3 IL-6 blockade–refractory iMCD-TAFRO patients. Cytokine panels, quantitative serum proteomics, flow cytometry of PBMCs, and pathway analyses were employed to identify novel therapeutic targets. To confirm elevated mTOR signaling, a candidate therapeutic target from the above assays, immunohistochemistry was performed for phosphorylated S6, a read-out of mTOR activation, in 3 iMCD lymph node tissue samples and controls. Proteomic, immunophenotypic, and clinical response assessments were performed to quantify the effects of administration of the mTOR inhibitor sirolimus.

Studies of 3 IL-6 blockade–refractory iMCD cases revealed increased $CD8^+$ T cell activation, VEGF-A, and PI3K/Akt/mTOR pathway activity. Administration of sirolimus substantially attenuated $CD8^+$ T cell activation and decreased VEGF-A levels. Sirolimus induced clinical benefit responses in all 3 patients with durable and ongoing remissions […]



# Identifying and targeting pathogenic PI3K/AKT/mTOR signaling in IL-6 blockade–refractory idiopathic multicentric Castleman disease

David C. Fajgenbaum,[1] Ruth-Anne Langan,[1] Alberto Sada Japp,[2] Helen L. Partridge,[1] Sheila K. Pierson,[1] Amrit Singh,[3] Daniel J. Arenas,[1] Jason R. Ruth,[4] Christopher S. Nabel,[5] Katie Stone,[6] Mariko Okumura,[7] Anthony Schwarer,[8] Fábio Freire Jose,[9] Nelson Hamerschlak,[10] Gerald B. Wertheim,[11] Michael B. Jordan,[12] Adam D. Cohen,[13] Vera Krymskaya,[1] Arthur Rubenstein,[1] Michael R. Betts,[2] Taku Kambayashi,[7] Frits van Rhee,[6] and Thomas S. Uldrick[14]

[1]Department of Medicine and [2]Department of Microbiology, Perelman School of Medicine, University of Pennsylvania, Philadelphia, Pennsylvania, USA. [3]Prevention of Organ Failure (PROOF) Centre of Excellence, Vancouver, British Columbia, Canada. [4]Castleman Disease Collaborative Network, Philadelphia, Pennsylvania, USA. [5]Dana Farber Cancer Research Institute, Boston, Massachusetts, USA. [6]Myeloma Institute, University of Arkansas for Medical Sciences, Little Rock, Arkansas, USA. [7]Department of Pathology & Laboratory Medicine, Perelman School of Medicine, University of Pennsylvania, Philadelphia, Pennsylvania, USA. [8]Department of Haematology and Oncology, Eastern Health Monash University Clinical School, Melbourne, Victoria, Australia. [9]Department of Rheumatology and [10]Department of Hematology, Hospital Israelita Albert Einstein, Sao Paulo, Brazil. [11]Department of Pathology & Laboratory Medicine, Children's Hospital of Philadelphia, Philadelphia, Pennsylvania, USA. [12]Division of Immunobiology, Department of Pediatrics, Cincinnati Children's Medical Center and University of Cincinnati College of Medicine, Cincinnati, Ohio, USA. [13]Abramson Cancer Center, University of Pennsylvania, Philadelphia, Pennsylvania, USA. [14]Fred Hutchinson Cancer Research Center, Seattle, Washington, USA.

**BACKGROUND.** Idiopathic multicentric Castleman disease (iMCD) is a hematologic illness involving cytokine-induced lymphoproliferation, systemic inflammation, cytopenias, and life-threatening multi-organ dysfunction. The molecular underpinnings of interleukin-6 (IL-6) blockade–refractory patients remain unknown; no targeted therapies exist. In this study, we searched for therapeutic targets in IL-6 blockade–refractory iMCD patients with the thrombocytopenia, anasarca, fever/elevated C-reactive protein, reticulin myelofibrosis, renal dysfunction, organomegaly (TAFRO) clinical subtype.

**METHODS.** We analyzed tissues and blood samples from 3 IL-6 blockade–refractory iMCD-TAFRO patients. Cytokine panels, quantitative serum proteomics, flow cytometry of PBMCs, and pathway analyses were employed to identify novel therapeutic targets. To confirm elevated mTOR signaling, a candidate therapeutic target from the above assays, immunohistochemistry was performed for phosphorylated S6, a read-out of mTOR activation, in 3 iMCD lymph node tissue samples and controls. Proteomic, immunophenotypic, and clinical response assessments were performed to quantify the effects of administration of the mTOR inhibitor sirolimus.

**RESULTS.** Studies of 3 IL-6 blockade–refractory iMCD cases revealed increased $CD8^+$ T cell activation, VEGF-A, and PI3K/Akt/mTOR pathway activity. Administration of sirolimus substantially attenuated $CD8^+$ T cell activation and decreased VEGF-A levels. Sirolimus induced clinical benefit responses in all 3 patients with durable and ongoing remissions of 66, 19, and 19 months.

**CONCLUSION.** This precision medicine approach identifies PI3K/Akt/mTOR signaling as the first pharmacologically targetable pathogenic process in IL-6 blockade–refractory iMCD. Prospective evaluation of sirolimus in treatment-refractory iMCD is planned (NCT03933904).

**FUNDING.** This study was supported by the Castleman's Awareness & Research Effort/Castleman Disease Collaborative Network, Penn Center for Precision Medicine, University Research Foundation, Intramural NIH funding, and the National Heart Lung and Blood Institute.

▶ Related Commentary: p. 4086

**Conflict of interest:** DCF is the index case. DCF receives research support from Janssen Pharmaceuticals. TSU is a coinventor on US patent 10,001,483 B2, assigned to the U.S. Government, with a portion of royalties going to employee-inventors under PL 99-502. TSU has research support through Cooperative Research and Development Agreements with the National Cancer Institute, Celgene Corporation, and Merck, and through a clinical trial agreement from Roche and the Fred Hutchinson Cancer Research Center.
**Role of funding source:** The funders had no role in study design, data collection and analysis, decision to publish, or preparation of the manuscript.

**Submitted:** November 8, 2018; **Accepted:** July 23, 2019; **Published:** September 16, 2019.
**Reference information:** *J Clin Invest*. 2019;129(10):4451–4463. https://doi.org/10.1172/JCI126091.

## Introduction

Multicentric Castleman disease (MCD) is characterized by polyclonal lymphoproliferation, hypervascularized lymph nodes containing dysmorphic germinal centers, cytokine-driven systemic inflammation, cytopenias, and multi-organ dysfunction. The estimated annual incidence of MCD in the USA is 1500–1800 and includes at least 2 subtypes (1). Kaposi sarcoma herpes virus (also known as human herpesvirus-8 [HHV-8]) is the etiologic agent (2) in 42%–67% of MCD cases, most commonly in the setting of HIV. The remaining MCD cases are HHV-8–negative and the etiology is idiopathic (iMCD) (3). International evidence-based consensus criteria for iMCD have been established and provide a framework for classifying iMCD and also describing the clinical and histopathologic variability in this disease (4). The most severe cases of iMCD often fall into the thrombocytopenia, anasarca, fever, reticulin fibrosis, and organomegaly (TAFRO syndrome) clinical subtype (5). The prognosis in iMCD is poor: 35% of patients die within 5 years of diagnosis, and 60% die within 10 years (6).

Several lines of evidence implicate elevated interleukin-6 (IL-6) in the pathogenesis of some cases of iMCD (7, 8). Blockade of IL-6 signaling with siltuximab, the only FDA-approved iMCD treatment, or tocilizumab, approved for iMCD treatment in Japan, can abrogate symptoms and improve lymphadenopathy (9, 10). These agents are recommended first-line in the treatment of iMCD (11). However, in the only randomized controlled trial performed of IL-6 blockade in iMCD, 66% of patients did not respond to therapy (10), and recent studies have not found significantly different serum IL-6 levels in iMCD patients compared with healthy controls (12). These observations indicate that other pathways may be driving disease pathogenesis in these patients. However, the pathological cell types, dysregulated signaling pathways, and driver cytokines in iMCD remain unknown. The limited understanding of etiology and pathogenesis has slowed drug development in iMCD and contributed to poor patient outcomes. iMCD patients refractory to IL-6 blockade are treated empirically with off-label treatment options, such as corticosteroids, rituximab, and cytotoxic chemotherapy, which have varying efficacies and significant toxicities (3). The most severe cases, often with the TAFRO clinical subtype, frequently require multi-agent cytotoxic chemotherapy (11). Identification of molecular and cellular abnormalities for therapeutic targeting is urgently needed for IL-6 blockade–refractory iMCD patients. However, no cell lines, animal models, or genomic, transcriptomic, or proteomic datasets of IL-6 blockade–refractory iMCD are available for high-throughput target identification. A precision medicine approach involving in-depth profiling of patient samples provides an opportunity for novel target identification.

Herein, we report the comprehensive evaluation of biospecimens from iMCD patients using proinflammatory cytokine panels, quantitative serum proteomics, flow cytometry of PBMCs, pathway analyses, and immunohistochemistry to identify a pharmacologically targetable disease pathway. Our results reveal increased $CD8^+$ T cell activation, VEGF-A levels, and PI3K/Akt/mTOR pathway activity during disease flare in 3 IL-6 blockade–refractory iMCD patients with the TAFRO subtype. PI3K/Akt/mTOR is a central pathway downstream of multiple cell surface receptors, including the T cell receptor (TCR) and VEGF receptor (13). PI3K/Akt/mTOR signaling is implicated in autoimmune (14) and malignant disorders (15) and is critical for cell proliferation, survival, and angiogenesis, including VEGF-A expression (13). Sirolimus is a potent mTOR inhibitor commonly prescribed for the prevention of organ transplant rejection but never reported in iMCD. We report for what we believe is the first time that administration of sirolimus induced significant cellular, proteomic, and clinical benefit responses in iMCD patients.

## Results

*Clinical description of 3 cases of IL-6 blockade–refractory iMCD.* Three iMCD patients who were refractory to IL-6 blockade and received multiple rounds of multi-agent cytotoxic chemotherapy presented to our care in need of a novel therapeutic approach. Clinical information is summarized in Table 1. In-depth target identification was performed in the index case (iMCD-1), and orthogonal methods for validation of candidate therapeutic targets and further target discovery were performed across all 3 patients (iMCD-1, iMCD-2, and iMCD-3) (Figure 1).

iMCD-1 is a 25-year-old male who initially presented in 2010 with a week-long history of constitutional symptoms, multicentric lymphadenopathy, and abdominal pain progressing rapidly to anasarca, organomegaly, thrombocytopenia, eruptive cherry hemangiomatosis, and multi-organ failure. Lymph node biopsy revealed histopathology consistent with iMCD, including notable hypervascularization (Supplemental Figure 1; supplemental material available online with this article; https://doi.org/10.1172/JCI126091DS1). Staining for HHV-8 was negative, and serum IL-6 was 6 pg/mL (normal: < 5 pg/mL). iMCD-1's clinicopathological features were consistent with the TAFRO clinical subtype of iMCD (4). Over 3.5 years, iMCD-1 experienced 5 acute disease flares and 8 prolonged hospitalizations (Figure 2A); the first 3 flares were previously reported (16). Of note, both corticosteroids and rituximab induced temporary partial improvements of symptoms for 1 month each, and bortezomib (velcade)-dexamethasone-thalidomide-adriamycin-cyclophosphamide-etoposide-rituximab (VDT-ACE-R) induced 15- and 16-month remissions before severe relapses. VDT-ACE-R was given to treat the fifth episode of multiple organ system failure, but further disease control and a new maintenance strategy were needed as all previous strategies (corticosteroids, rituximab, siltuximab, VDT-siltuximab) failed to prevent relapse.

iMCD-2 is a female who presented at 17 years of age with severe constitutional symptoms, effusions, cytopenias, renal dysfunction, hypoalbuminemia, and multicentric lymphadenopathy with iMCD histopathology, including hypervascularization (Table 1, Supplemental Figure 1). She was diagnosed with the TAFRO subtype of iMCD and initially treated with doxorubicin-bleomycin-vinblastine-dacarbazine combination chemotherapy and tocilizumab, which induced a clinical response. Tocilizumab was continued for maintenance. Two and a half years after beginning tocilizumab, she had a disease recurrence involving anemia, fatigue, arthralgia, and generalized lymphadenopathy. An alternative to cytotoxic chemotherapy to induce remission was desired.

iMCD-3 is a female who presented at 61 years of age with nausea, vomiting, constitutional symptoms, lymphadenopathy, fluid retention, renal failure requiring hemodialysis, and pulmonary failure requiring mechanical ventilation. A lymph

**Table 1. Demographics, disease history, and treatment history for iMCD-1, iMCD-2, iMCD-3**

| | iMCD-1 | iMCD-2 | iMCD-3 |
|---|---|---|---|
| **Demographics and diagnosis** | | | |
| Sex | M | F | F |
| Race | White | Indian | White |
| Age at diagnosis | 25 | 17 | 61 |
| Diagnosis (clinical subtype) | iMCD (TAFRO) | iMCD (TAFRO) | iMCD (TAFRO) |
| Multicentric lymphadenopathy (> 1 cm) | Y, disseminated | Y, disseminated | Y, disseminated |
| Pathology consistent with diagnostic criteria (4), subtype | Y, hypervascular/ hyaline vascular | Y, hypervascular/ hyaline vascular | Y, hypervascular/ hyaline vascular |
| Histopathology grades (0–3): | | | |
| Atrophic germinal centers | 1 | 3 | 3 |
| FDC prominence | 1 | 2 | 2 |
| Vascularity | 3 | 2 | 3 |
| Plasmacytosis | 2 | 1 | 1 |
| Hyperplastic germinal centers | 1 | 0 | 0 |
| Diseases excluded, per criteria | Y | Y | Y |
| **Clinical features and nadir laboratory values at diagnosis** | | | |
| Constitutional symptoms | Y | Y | Y |
| Anasarca | Y | Y | Y |
| Organomegaly | Y (HSM) | Y (HM) | Y (SM) |
| C-reactive protein (mg/L) | 302 (< 7.6) | 99 (< 5) | 251 (< 3) |
| IgG (mg/dL) | 930 (650–1850) | 810 (700–1400) | NR |
| Hemoglobin (g/dL) | 6.8 (13.5–15) | 6.4 (12–15) | 6.4 (12.0–15.5) |
| Platelet count (k/μL) | 15 (150–400) | 84 (150–400) | 21 (150–450) |
| Albumin (g/dL) | 1.2 (3.5–5) | 1.6 (3.4–4.7) | 2.8 (3.5–5.5) |
| Creatinine (mg/dL) | 2.55 (0.7–1.3) | 1.67 (0.45–1.02) | 2.14 (0.5–1.0) |
| IL-6 (pg/mL) | 6 (< 5) | NR | 75.9 (< 7) |
| **Treatment history** | | | |
| Treatment course | methylprednisolone, rituximab, VDT-ACE-R-IVIg-siltuximab, tocilizumab-pentoxifylline-ciprofloxacin-VDT-siltuximab, celecoxib-VDT-siltuximab, cyclosporin-IVIg-VDT-siltuximab, VDT-ACE-R-IVIg, sirolimus-IVIg | prednisone, doxorubicin-bleomycin-vinblastine-dacarbazine-dexamethasone, tocilizumab, sirolimus | methylprednisolone-tocilizumab-rituximab, sirolimus |
| Reason for discontinuing IL-6 blockade | lack of efficacy, recurrence of symptoms on therapy | loss of adequate response/recurrence of symptoms on therapy | loss of adequate response/recurrence of symptoms on therapy |

HM, hepatomegaly; HSM, hepatosplenomegaly; IVIg, intravenous immunoglobulin; NR, not recorded; SM, splenomegaly; VDT-ACE-R, velcade-dexamethasone-thalidomide-adriamycin-cyclophosphamide-etoposide-rituximab; TAFRO, thrombocytopenia, anasarca, fever/elevated C-reactive protein, renal dysfunction, myelofibrosis, organomegaly.

node biopsy demonstrated iMCD histopathology and was noted to have increased vascularization (Table 1, Supplemental Figure 1). Her clinical features were consistent with the TAFRO subtype of iMCD. She received rituximab and tocilizumab, which induced a clinical response, and was maintained on tocilizumab for 2 years. Then, she experienced recurrence of fatigue, anasarca, splenomegaly, and lymphadenopathy while on tocilizumab.

Although iMCD is considered an IL-6–driven disorder, IL-6 blockade failed to induce a response during 3 flares for iMCD-1 and failed to prevent relapses in all 3 patients. The lack of response to IL-6 blockade in these patients and others strongly suggests that additional signaling pathways may be important to disease pathogenesis in a portion of patients.

*Identification of a candidate therapeutic target*. To identify additional candidate therapeutic targets for IL-6 blockade–refractory iMCD, we performed a series of molecular and cellular immunological studies, beginning with iMCD-1, who had extensive clinical data and biospecimens available. Analyses of 13 serum inflammatory markers measured in the months preceding iMCD-1's fifth flare revealed that levels of soluble IL-2 receptor alpha chain (sIL-2Rα), a marker of T cell activation, rose above the upper limits of normal (ULN) 20 weeks before onset of flare and peaked at 10-fold above the ULN during flare (Figure 2B). sIL-2Rα levels were also 3- to 4-fold above the ULN when measured during 2 previous flares. Our analyses of 13-analyte inflammatory marker data measured in the months preceding the fifth flare identified VEGF-A as the only other inflammatory marker that rose above the ULN before flare. VEGF-A levels approached the ULN 8 weeks before the flare and peaked at 3-fold above the ULN during flare (Figure 2B). VEGF-A levels were also 2- to 4-fold above the ULN when measured during 2 previous flares. This

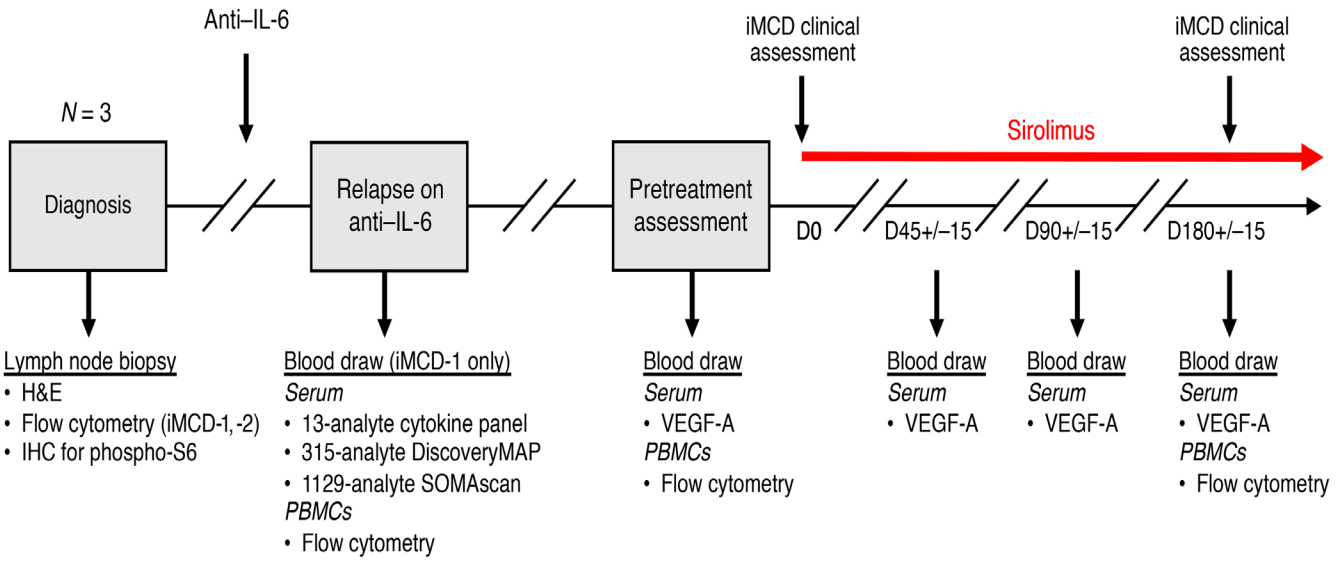


**Figure 1. Study schema.** Flow of 3 IL-6 blockade–refractory iMCD patients (iMCD-1, iMCD-2, iMCD-3) with TAFRO syndrome for whom translational studies were performed and sirolimus was administered. Sirolimus trough was maintained at 5–10 ng/mL. iMCD clinical assessment included MCD Overall Symptom Score, Clinical Benefit Response, and Cheson Criteria.

observation is consistent with iMCD-1's VEGF-A–associated clinicopathological manifestations — cherry hemangiomatosis, capillary leak syndrome, and lymph node hypervascularization. None of the other 11 clinically measured serum inflammatory markers demonstrated a consistent upward trend prior to flare onset (Supplemental Figure 2).

Based on the longitudinal measurement of select serum inflammatory markers, serum-based proteomics was next pursued to screen a larger panel of analytes for differential expression between flare and remission in order to identify additional candidate targets. The Myriad-RBM DiscoveryMAP proteomic platform, which quantifies the levels of 315 analytes, revealed that sIL-2Rα and VEGF-A were 2 of the most elevated serum proteins at the onset of both flares for which samples were available compared with a remission sample. sIL-2Rα was 5-fold (average $\log_2$ [flare/remission]: 2.38) greater in flare than remission and the 15th most upregulated analyte (Figure 3A and Supplemental Table 1). VEGF-A was the most upregulated cytokine and the sixth most upregulated analyte (average $\log_2$ [flare/remission]: 3.52) during flare (Figure 3A and Supplemental Table 1). The longitudinal changes preceding disease flare and upregulation in sIL-2Rα and VEGF-A during flares suggested a possible pathogenic role for T cell activation and VEGF-A in iMCD-1's disease flares.

To identify candidate targetable pathways central to both T cell activation and VEGF-A expression, we performed enrichment analysis of DiscoveryMAP data for analytes with a $\log_2$-fold change greater than 2 during flare. Analysis using the Kyoto Encyclopedia of Genes and Genomes (KEGG) database identified 35 and 33 significant pathways (FDR < 0.01) for iMCD-1's third and fifth flares, respectively. PI3K/Akt signaling was the only signaling pathway in the top 5 most-enriched pathways for both flares and the only signaling pathway identified that included both sIL-2Rα and VEGF-A (Figure 3, B and C and Supplemental Table 2). We then sought to identify drug classes that decrease expression in vitro of the elevated analytes identified through DiscoveryMAP; enrichment analysis using the Library of Integrated Network-based Cell Signature 1000 database identified 17 unique compounds with FDR < 0.01 that were likewise predicted to decrease VEGF-A expression (Supplemental Table 3). Compounds inhibiting PI3K/Akt/mTOR were the most represented (5 compounds). Two compounds target MEK and the remaining each had unique targets (Supplemental Table 3). These results indicated that PI3K/Akt/mTOR may be a targetable pathway linking T cell activation and VEGF-A expression. To discover additional candidate pathways, we used an orthogonal proteomics platform, SomaLogic SOMAscan, which measures 1129 analytes, to analyze plasma samples obtained at the same time as those analyzed by DiscoveryMAP. Ingenuity Pathway Analysis of analytes with at least a 2-fold change ($\log_2$ [flare/remission] ≥ 1) between flare and remission identified canonical pathways associated with PI3K/Akt/mTOR signaling as top pathways for both flares (Supplemental Table 4 and Supplemental Table 5). Together, these 3 separate analyses triangulated on PI3K/Akt/mTOR signaling as a candidate pathway central to the increased T cell activation and VEGF-A expression identified through serum proteomics.

*Investigation and inhibition of a candidate therapeutic target.* Next, we investigated whether the candidate therapeutic targets identified from proteomic analyses in iMCD-1 were present across all 3 cases (iMCD-1, iMCD-2, iMCD-3). To determine if there was increased T cell activation during disease flare in the 3 IL-6 blockade–refractory patients, we performed flow cytometry on PBMCs obtained from all 3 patients during relapse and 3 age-matched healthy controls. These analyses revealed a significantly decreased $CD4^+/CD8^+$ T cell ratio (Supplemental Figure 3) and a significantly increased proportion of $CD38^+$ (activated) $CD8^+$ T cells during flare compared with healthy controls (Figure 4, A and B). Activated $CD8^+$ T cells coexpressing CD38 and HLA-DR also trended higher in patients during flare compared with controls ($P$ = 0.0513) (Figure 4, A and C) (16). The increased T cell activation observed by flow cytometry is consistent with proteomic findings

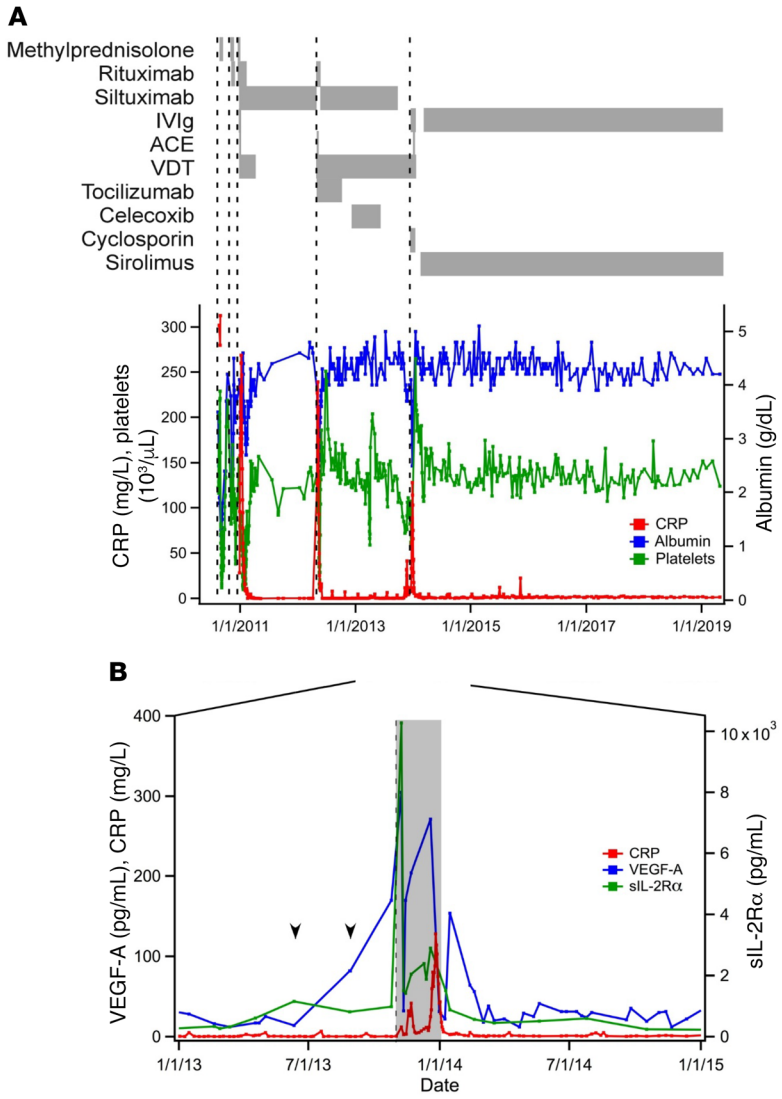


**Figure 2. Clinical course and elevation of VEGF-A and sIL-2Rα prior to disease flare for iMCD-1.** (**A**) Select laboratory values, dates of initiation of disease flares (dotted vertical lines; defined by hypoalbuminemia (< 3.5 g/dL), elevated CRP (> 10 mg/L), anemia (hemoglobin < 13.5 g/dL), renal dysfunction (creatinine > 1.3 mg/dL), constitutional symptoms, and fluid accumulation), and treatment regimens administered throughout iMCD-1's disease course ($n$ = 1). CRP closely parallels disease status. IVIg, intravenous immunoglobulin; ACE, doxorubicin (adriamycin)-cyclophosphamide-etoposide; VDT, bortezomib (velcade)-dexamethasone-thalidomide; CRP, C-reactive protein. (**B**) Serum levels of sIL-2Rα (normal < 1022 pg/mL) and VEGF-A (normal < 86 pg/mL) from 1 year before to 1 year after iMCD-1's fifth disease flare (onset indicated by dotted vertical line; duration by shaded region), with CRP included for reference. Arrows indicate when sIL-2Rα and VEGF-A rose above the ULN.

and specific to CD8⁺ T cells as no differences were observed in CD4⁺ T cell populations (data not shown).

In 2 patients (iMCD-1, iMCD-2), the proportions of CD4⁺ and CD8⁺ T cells were also measured in lymph node tissue by flow cytometry as part of their clinical evaluations. No statistical tests could be performed to compare these cases against normal lymph node proportions due to the sample size of 2; the mean and SD of a historic normal control group are provided for reference (17). Consistent with what was seen in circulation, the proportions of CD8⁺ T cells were higher in both cases (iMCD-1: 29%; iMCD-2: 15%) than the mean plus 1 SD in a historic normal control group: 10% ± 3.3% (17). The proportions of CD4⁺ T cells (iMCD-1: 32%; iMCD-2: 17%) and CD4⁺/CD8⁺ T cell ratios (iMCD-1: 1.1; iMCD-2: 1.1) were lower in both cases than the mean minus 1 SD in a historic normal control group: 48% ± 12.8% and 4.5 ± 1.38, respectively (17). The increased proportion of CD8⁺ T cells relative to CD4⁺ T cells in circulation and lymph node is consistent with an expanding population of activated CD8⁺ T cells.

To determine if iMCD-2 and iMCD-3 had elevated circulating VEGF-A levels similar to iMCD-1 (348 pg/mL) during relapse, serum VEGF-A levels were measured for both patients at the time of relapse. iMCD-2's VEGF-A level (165 pg/mL) was approximately 2 times the ULN (86 pg/mL), and iMCD-3's VEGF-A level (1727 pg/mL) was greater than 20-fold above the ULN (Figure 4D). As was observed with iMCD-1, iMCD-2 and iMCD-3 also demonstrated clinicopathologic features associated with elevated VEGF-A, such as hypervascularized lymph nodes (Supplemental Figure 1) and capillary leak syndrome. The average lymph node vascularity score (average: 2.67/3) for these 3 cases was the highest score among the 5 histopathological features (atrophic germinal centers, plasmacytosis, vascularity, hyperplastic germinal centers, follicular dendritic cell prominence) graded by a panel of expert hematopathologists (Table 1).

Based on the shared features of increased CD8⁺ T cell activation and circulating VEGF-A levels across all 3 cases and the identification of PI3K/Akt/mTOR signaling as a candidate central signaling pathway underlying these abnormalities in iMCD-1, we hypothesized that PI3K/Akt/mTOR signaling would be increased in patients' lymph node tissue. We quantified levels of phosphorylated ribosomal protein S6 (phospho-S6), a read-out for mTOR activity (18), in diagnostic lymph node tissue from all 3 cases to determine if PI3K/Akt/mTOR signaling is elevated during disease flare. Nonspecific reactive and autoimmune lymphoproliferative syndrome (ALPS) lymph nodes were included as comparators. Reactive nodes were chosen to reflect lymphoproliferation due to a nonspecific immune reaction, whereas ALPS was chosen as a positive control because it has clinical and lymph node histopathological overlap with iMCD (19), involves pathologically increased PI3K/Akt/mTOR activity (14), and responds clinically to mTOR inhibition (20). Quantification of positive staining proportions revealed that phospho-S6 is significantly and specifically elevated in the interfollicular space of all 3 IL-6 blockade–refractory iMCD-TAFRO cases, but not in the germinal centers, compared with reactive nodes (Figure 4, E–I). Further, phospho-S6 expression levels in these iMCD-TAFRO cases are similar in magnitude and distribution to those observed in ALPS, a disease known to involve hyperactive mTOR signaling (14) and for which mTOR inhibition is standard of care (20). These findings confirm that the activity of the PI3K/Akt/mTOR path-

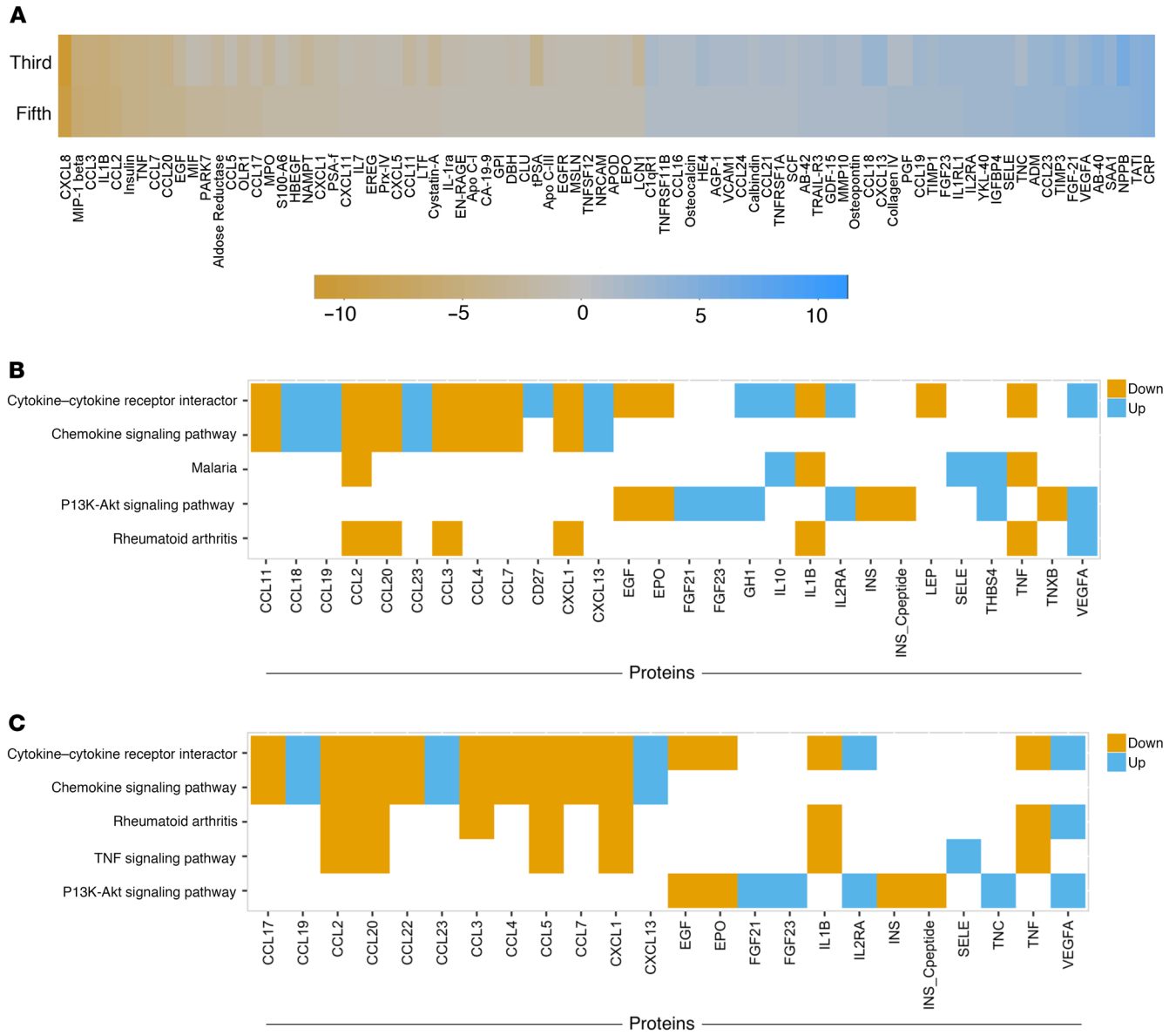


**Figure 3. Serum proteomics and pathway analyses identify VEGF-A, sIL-2Rα, and PI3K/Akt/mTOR signaling as candidate therapeutic targets for iMCD-1.** (**A**) Heatmap of the analytes whose levels increase (blue) or decrease (orange) by at least 2-fold in the same direction between flare and remission for iMCD-1's third and fifth flares, as measured by Myriad RBM DiscoveryMAP ($n$ = 1). Analytes are presented in ascending order from left to right based on the $\log_2$ (flare/remission) fold-change at the fifth flare, compared with remission. Key provides the color intensity for a given fold change. (**B**, **C**) Enrichment analysis, using Enrichr, of Myriad RBM DiscoveryMAP gene sets for metabolic pathways for iMCD-1. Results of the top 5 enriched gene sets (FDR < 0.01, rank ordered by combined score) from the (**B**) third flare and (**C**) fifth flare when proteins with $\log_2$ (flare/remission) greater than 2 were analyzed for KEGG pathway gene sets. Colored cells represent gene members in specific pathways that were found to be greater than 4-fold up (blue) or 4-fold down (orange) during flare compared with remission.

way is increased in iMCD-TAFRO cases and suggests that PI3K/Akt/mTOR signaling may be a pathogenic mechanism in IL-6 blockade–refractory iMCD-TAFRO.

Given these findings and that these patients had relapsed on prior regimens, all 3 patients were started on the mTOR inhibitor sirolimus (3 mg/day), an immunomodulatory and antiproliferative drug and what we believe to be a novel therapy for iMCD. Dosing was modulated to achieve trough levels of 5–10 ng/mL, consistent with dosing for ALPS (20). The 3 patients experienced a significant decline in activated $CD8^+$ T cells between pretreatment flare samples and remission samples on sirolimus (Figure 5, A–C), similar to levels found in age-matched healthy controls. Following initiation of sirolimus, VEGF-A levels remained in the normal range for iMCD-1 (Figure 2A), trended slightly downwards in iMCD-2 (Figure 5D), and declined dramatically in iMCD-3 from 20-fold above the ULN to within the normal range (Figure 5E).

These cellular and molecular changes corresponded with achievement of durable symptomatic response (10) and clinical benefit response criteria (21) for all 3 patients, using 2 dif-

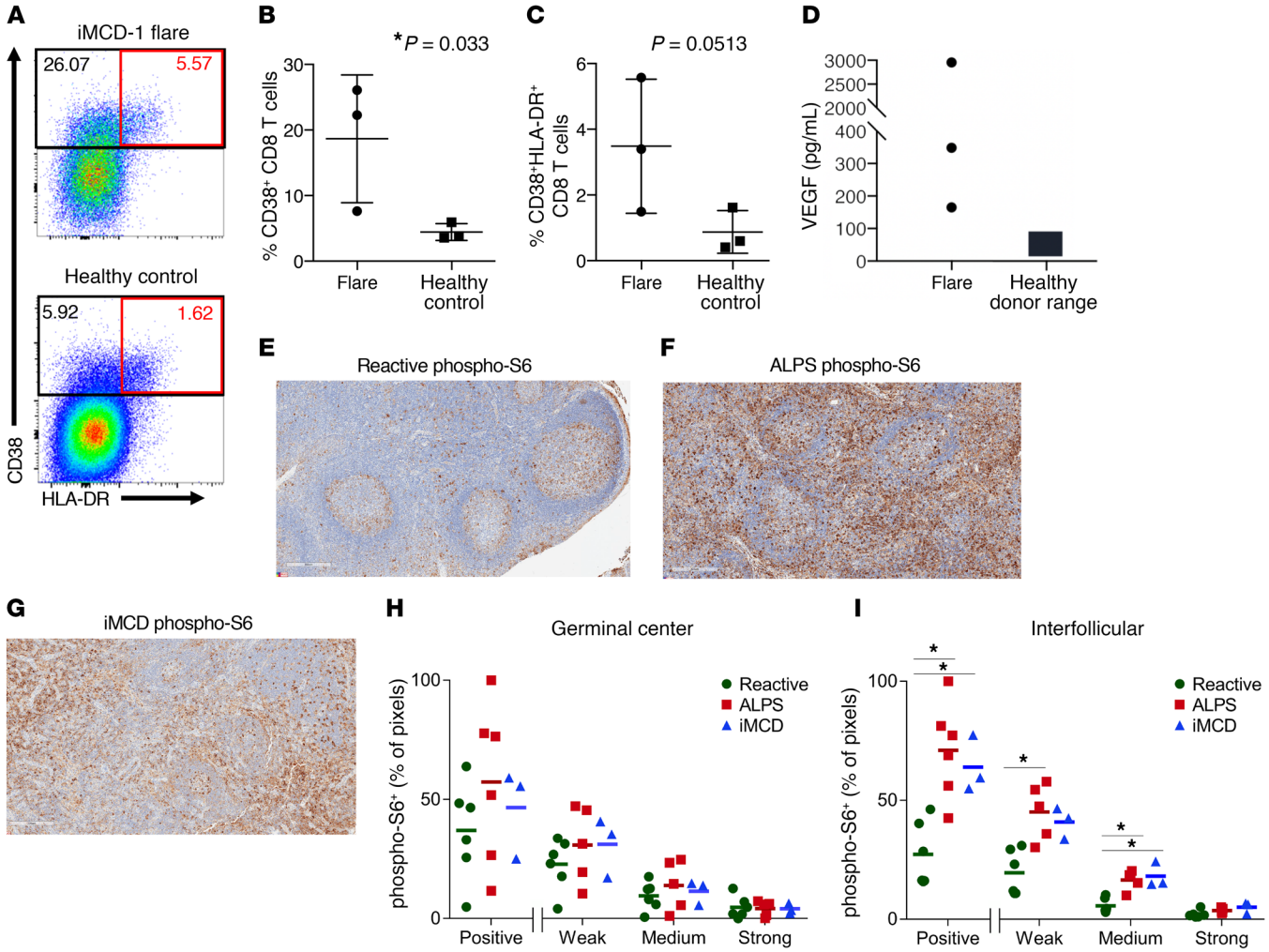


**Figure 4. Increased CD8⁺ T cell activation, VEGF-A levels, and mTOR signaling in IL-6 blockade–refractory iMCD.** (**A**–**C**) Flow cytometry of PBMCs gated for live nonnaive CD8⁺ T cells. PBMCs were obtained from iMCD-1, iMCD-2, and iMCD-3 at onset of a relapse of flare ($n$ = 3, represented by iMCD-1 flare), and from 3 age-matched healthy controls (Healthy control). Nonnaive CD8⁺ T cells were gated for expression of CD38 and HLA-DR. The percentage of cells within the gated regions is provided for each (black rectangle: CD38⁺; red rectangle: CD38⁺HLA-DR⁺). Mean with SEM is presented. Unpaired 1-tailed Student's $t$ test was performed between the 3 iMCD flare samples and 3 age-matched healthy controls. No abnormalities were observed in the CD4⁺ T cell population (data not shown). (**D**) Circulating VEGF-A levels were measured for iMCD-1 and iMCD-3 at the time of relapse as part of routine clinical care; VEGF-A for iMCD-2 was measured with a clinical grade assay (ARUP Laboratories) ($n$ = 3). Healthy control range (9–86 pg/mL) is shown. (**E**–**I**) Immunohistochemistry was performed on lymph node tissue and representative images are provided of a reactive (Reactive) (**E**), an autoimmune lymphoproliferative syndrome (ALPS) (**F**), and an iMCD (iMCD) (**G**) lymph node immunostained (brown) in parallel with an antibody against phosphorylated ribosomal protein S6 (phospho-S6), a marker of mTOR activation, and counterstaining with hematoxylin (blue) (scale bars: 300 μm). (**H**) Quantification of germinal center staining intensity and (**I**) quantification of interfollicular staining intensity, shown as the percentage of pixels stained positive, as well as the breakdown of weak, medium, or strong staining, for reactive (green circle; $n$ = 6), ALPS (red square; $n$ = 5), and iMCD (blue triangle; $n$ = 3). Dot plots along with the means are presented. Statistical significance was tested by comparing the centered log-transformed ratios by a 1-tailed Mann-Whitney $U$ test. *$P < 0.05$.

ferent previously published criteria for assessing response in iMCD (Table 2). iMCD-1, iMCD-2, and iMCD-3 met the durable symptomatic response criteria of at least a 50% improvement in MCD-related Overall Symptom Score (MCD-OSS) (10) with changes in MCD-OSS from presirolimus of –100%, –66%, and –75%, respectively (Figure 5F). Responses are durable and ongoing in iMCD-1, iMCD-2, and iMCD-3, as of July 2019, for 66, 19, and 19 months, respectively. Both patients (iMCD-2 and iMCD-3) for which lymphadenopathy was present and a lymph node/tumor response could be assessed by Cheson criteria (22) obtained a complete response. Due to rapid clinical deterioration, iMCD-1 had received multi-agent cytotoxic chemotherapy, which induced a complete lymph node/tumor response and partial clinical response, prior to beginning sirolimus, making it impossible to assess lymph node/tumor response criteria with regard to sirolimus. Following chemotherapy, iMCD-1 had low-grade persistent symptoms with an MCD-OSS of 6 before sirolimus was started. However, with continuous sirolimus and immuno-repletive dosing of intravenous immunoglobulin (IVIg) (500 mg/kg/month) for rituximab-associated hypogammaglobulinemia, iMCD-1 has been in a 66-month complete remission as of July 2019, 8 times longer than the average of the previous remission durations (7.6 months), which had also been induced by multi-agent chemotherapy and previously maintained with IL-6 blockade and chemo-

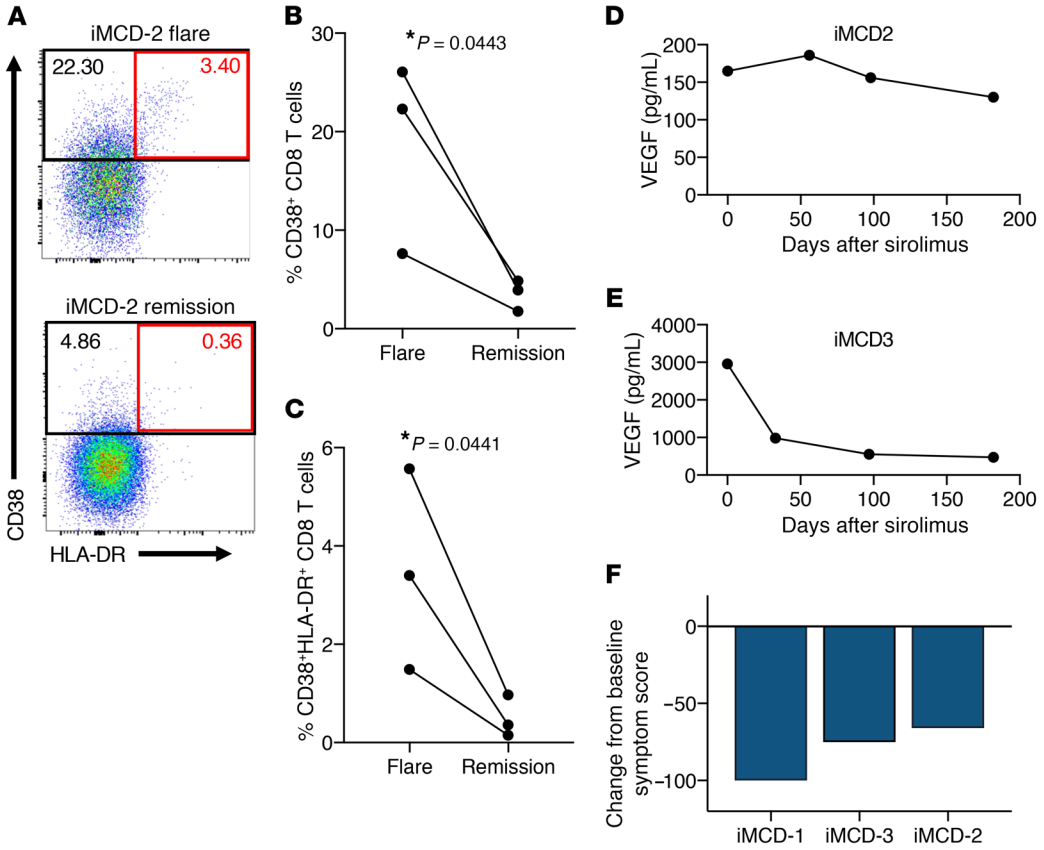


**Figure 5. Decreased T cell activation and VEGF-A levels following therapeutic inhibition of mTOR in IL-6 blockade–refractory iMCD.** (**A**–**C**) Flow cytometry of PBMCs gated for live nonnaive CD8$^+$ T cells. PBMCs from iMCD-1, iMCD-2, and iMCD-3 at onset of a relapse of flare ($n$ = 3, represented by iMCD-2 flare), as per Figure 4A–C, were compared with PBMCs after a remission was achieved with mTOR inhibition for all 3 patients (represented by iMCD-2 remission). Nonnaive CD8$^+$ T cells were gated for expression of CD38 and HLA-DR. The percentage of cells within the gated regions is provided for each (black rectangle: CD38$^+$; red rectangle: CD38$^+$HLA-DR$^+$). Paired 1-tailed Student's $t$ test was performed between the 3 iMCD flare samples and 3 remission samples, $P < 0.05$. (**D**–**E**) Circulating VEGF-A levels were measured by a clinical grade assay (ARUP Laboratories) for iMCD-2 (**D**) and as part of routine clinical care for iMCD-1 (data presented in Figure 2B) and iMCD-3 (**E**) at the time of relapse and at 3 subsequent time points after sirolimus was initiated. Healthy control range for both VEGF-A assays was 9–86 pg/mL. (**F**) Plot displaying the percentage change in baseline symptom score as determined by the MCD-related overall symptoms score for iMCD-1, iMCD-2, and iMCD-3 ($n$ = 3).

therapy. Both VEGF-A and sIL-2Rα remained in the normal range for the last 66 months (data not shown).

Transition of therapy from tocilizumab to sirolimus monotherapy in the midst of a mild relapse of disease activity (MCD-OSS: 12) for iMCD-2 resulted in improved hemoglobin levels, fatigue, anorexia, and arthralgia, and shrinkage of enlarged lymph nodes. The patient has felt well enough to return to full-time university coursework. Replacement of tocilizumab with sirolimus monotherapy during a moderate relapse of disease activity (MCD-OSS: 24) for iMCD-3 relieved fatigue and splenomegaly, lessened fluid accumulation, and shrank lymph node size. All 3 patients report feeling well on sirolimus with no relapses and no significant complications. While iMCD-1 initially experienced oral ulcers as a side effect, they resolved after 4 months. These results indicate that PI3K/Akt/mTOR is an actionable therapeutic target and that sirolimus is capable of extending remission and abrogating disease activity in IL-6 blockade–refractory iMCD.

## Discussion

iMCD is widely considered an IL-6–driven disorder. However, IL-6 is not uniformly elevated in iMCD, and IL-6 blockade is effective in only a portion of cases. Comprehensive investigation of clinical, cellular, and molecular data identified activated CD8$^+$ T cells and elevated VEGF-A as hallmarks of iMCD disease flares and PI3K/Akt/mTOR as a therapeutic target, linking T cell activation and VEGF-A in iMCD for the first time. Taken together, the findings presented here suggest that sirolimus administration is effective for both maintaining disease remission and treating disease flare in IL-6 blockade–refractory iMCD-TAFRO.

Sirolimus is FDA-approved for the prevention of renal allograft rejection (23) and treatment of lymphangioleiomyomatosis (24) and has an established long-term safety profile. Compared with existing chemotherapies and other targeted therapies that could have been trialed off-label for these patients, sirolimus is inexpensive, available as a convenient oral formulation, and well tolerated. Multiple mechanisms of action reported for sirolimus in other conditions may contribute to the therapeutic efficacy observed in iMCD (23). Data from this study support a model in which sirolimus' efficacy is asserted through inhibition of mTOR, CD8$^+$ T cell activation, cytokine secretion (including VEGF-A), and cell proliferation (13) (Supplemental Figure 4). Several lines of evidence implicate PI3K/Akt/mTOR pathway activi-

**Table 2. Clinical and laboratory features before and after sirolimus administration and clinical benefit responses for iMCD-1, iMCD-2, and iMCD-3**

| | iMCD-1[A] | | iMCD-2 | | iMCD-3 | |
|---|---|---|---|---|---|---|
| **Clinical features pre/post sirolimus** | | | | | | |
| | Pre | Post | Pre | Post | Pre | Post |
| Constitutional symptoms | Y (grade 2 fatigue, night sweats) | N | Y (grade 3 fatigue) | Y (grade 1 fatigue) | Y (grade 2 fatigue) | Y (grade 1 fatigue) |
| Anasarca | N | N | N | N | Y | N |
| Organomegaly | N | N | N | N | Y | N |
| Multicentric lymphadenopathy | N | N | Y | N | Y | N |
| MCD-related Overall Symptom Score[B] | 6 | 0 | 12 | 4 | 24 | 6 |
| **Clinical benefit response criteria** | | | | | | |
| A 2 g/dL increase in hemoglobin without transfusions | NA[A] | | Y | | NA | |
| A 1 grade[C] decrease in fatigue | Y | | Y | | Y | |
| A 1 grade[C] decrease in anorexia | NA[A] | | Y | | Y | |
| A 2°C decrease in fever or return to 37°C or improvement in night sweats | Y | | NA | | NA | |
| A 5% increase in weight, if significant weight loss occurred with disease | NA[A] | | Y | | NA | |
| A 25% decrease bidimensionally in size of the largest lymph node | NA[A] | | Y | | Y | |
| Clinical benefit response[D] | Y | | Y | | Y | |
| **Durable symptomatic and tumor/lymph node response** | | | | | | |
| % change in MCD-related Overall Symptom Score[B] | −100% | | −66% | | −75% | |
| Durable symptomatic response[E] | Y | | Y | | Y | |
| Tumor/lymph node response[F] | NA[A] | | CR | | CR | |
| Duration on sirolimus without relapse | 66 months, ongoing | | 19 months, ongoing | | 19 months, ongoing | |

[A]iMCD-1 received multiagent chemotherapy, which induced a partial symptomatic response and complete lymph node response, before beginning sirolimus. Therefore, improvement in hemoglobin, anorexia, weight, decrease in lymph node size, and tumor/lymph node response are not applicable (NA), because they were not present when sirolimus was commenced. [B]MCD-related Overall Symptom Score was developed for the phase II clinical trial of siltuximab (10). It involves assessing 34 clinical features according to the National Cancer Institute Common Terminology Criteria of Adverse Events (NCI CTCAE), version 3.0, and adding up the grades for each. [C]According to the NCI CTCAE, version 3.0. [D]Developed for the phase I siltuximab clinical trial (21), clinical benefit response requires an improvement from baseline in at least one of the above criteria without worsening in the other measures. [E]Developed for the phase II siltuximab clinical trial (10), a ≥50% reduction in overall MCD-related Overall Symptom Score sustained for at least 18 weeks, according to 34 MCD-related signs and symptoms. [F]According to revised Cheson criteria (22) that was utilized in the phase II siltuximab clinical trial.

ty as being critical to VEGF-A expression (25–29) and T cell activation (30–33), and mTOR inhibition exerts the expected effect of inhibiting these functions. Sirolimus may also be acting on cell types other than T cells, such as macrophages (34), which could also contribute to elevated VEGF-A levels, and regulatory T cells, which sirolimus relatively spares the function and proliferation of compared with effector T cells. Several other diseases involving immune dysregulation, including ALPS and systemic lupus erythematosus, are known to involve increased PI3K/Akt/mTOR pathway activation and benefit from sirolimus (14, 35). In ALPS, sirolimus abrogates survival and proliferation of disease-driving double-negative T cells and their precursors (14). Importantly, we demonstrated that phospho-S6 was increased in the 3 iMCD patients to a similar level as the ALPS cases. In patients with lupus who respond to sirolimus, sirolimus significantly decreases effector memory $CD8^+$ T cells, decreases proinflammatory T cells, and increases regulatory T cells (35). Investigations into the cell types expressing phospho-S6 in these cases were not performed. Future studies involving immunofluorescence or flow cytometry are needed to identify these cell types in iMCD. While mTOR signaling may or may not be the primary driver in iMCD, the improvement in symptoms in these patients suggest that it is critical to pathogenesis.

In addition to therapeutic markers, sIL-2Rα, VEGF-A, and $CD38^+CD8^+$ T cells may be important markers for monitoring disease status in iMCD. sIL-2Rα and VEGF-A rose above the ULN weeks before symptom onset in iMCD-1. An analysis of iMCD case studies found elevated sIL-2Rα and VEGF-A in 20 of 21 and 16 of 20 cases, respectively (3), a finding confirmed by subsequent serum proteomics studies (12, 36). The activated $CD38^+CD8^+$ T cells, which were increased in the 3 iMCD patients and decreased with sirolimus, are also expanded in HIV (37) and systemic lupus erythematosus and likewise decrease with effective disease control (38). Further research is needed to investigate the usefulness of these markers and others in larger cohorts and their potential predictive and therapeutic implications. A large-scale serum proteomics study is currently underway.

There are several limitations to this study. First, this study included only 3 iMCD patients. Despite the small sample size, the levels of well-established biological targets of sirolimus were significantly increased compared with controls and also showed significant decline following sirolimus treatment, suggesting

a robust biological response. Second, all 3 patients exhibit the TAFRO syndrome clinical subtype of iMCD, and they were not selected at random. Sirolimus was administered to these patients because they shared clinicopathological features and cellular and molecular findings suggesting mTOR inhibition may be effective. Furthermore, 2 of the patients (iMCD-2 and iMCD-3) had a gradual reemergence of symptoms, providing a window of time to attempt sirolimus before chemotherapy would be indicated. Therefore, these findings may only be limited to IL-6 blockade–refractory iMCD patients with TAFRO syndrome; a larger clinical trial is needed to assess efficacy across iMCD patients and identify potential biomarkers of response. Based on our data, a clinical trial of sirolimus in IL-6 blockade refractory iMCD will begin enrollment in August 2019 (NCT03933904). Third, iMCD-1 had already received cytotoxic chemotherapy before sirolimus was administered, and he receives immunorepletive dosing of IVIg, which can demonstrate a variety of immunomodulatory mechanisms at higher doses (39), concurrently with sirolimus, limiting the ability to fully assess the impact of sirolimus in this case. However, iMCD-1's prolonged remission as well as durable symptomatic and lymph node responses in iMCD-2 and iMCD-3 in the midst of more severe disease suggest that sirolimus is active. Fourth, the etiology of the increased PI3K/Akt/mTOR signaling in these cases is unknown. A clinical whole exome sequencing analysis (Baylor College of Medicine, Dallas, TX) of DNA from PBMCs from iMCD-1 was performed to identify a mutation or variant related to the patient's phenotype, but none were found. Genetic sequencing of germline DNA and lymph node tissue DNA is in process in other patients, but has also failed to identify a clear genomic driver to date. Extensive viral discovery across lymph node tissue from 11 iMCD patients also failed to reveal an acute viral infection as the etiology of iMCD (40). Auto-antibody screening is currently underway to identify circulating self-reactive antibodies that could initiate inflammatory signaling. Though the etiology of the increased PI3K/Akt/mTOR activation is unknown, this study demonstrates the potential for cellular, proteomic, and molecular assays to identify therapeutic targets that can lead to patient benefit even while the etiology remains unknown.

The precision medicine approach employed implicates activated $CD8^+$ T cells, PI3K/Akt/mTOR signaling, and VEGF-A in iMCD pathogenesis and suggests that sirolimus may be an effective treatment for refractory iMCD.

## Methods

*Clinical and laboratory data*. All laboratory values, treatments, and sample collection dates were obtained from the patients' medical records. Dates of disease flares in Figure 2A were defined by hypoalbuminemia (< 3.5 g/dL), elevated C-reactive protein (CRP) (> 10 mg/L), anemia (hemoglobin < 13.5 g/dL), renal dysfunction (creatinine > 1.3 mg/dL), constitutional symptoms, and fluid accumulation. All laboratory tests were performed in hospital laboratories or in Clinical Laboratory Improvement Amendments of 1988–certified (CLIA-certified) laboratories. sIL-2Rα data for iMCD-1 were averaged when multiple tests were performed on a single day. VEGF-A levels were obtained from medical record data for iMCD-1 and iMCD-3. VEGF-A levels were not quantified through clinical testing for iMCD-2, so samples were sent to ARUP Laboratories for testing. The circulating VEGF-A normal range was less than 86 pg/mL for all assays. Data from flow cytometry of lymph node tissue (iMCD-1 and iMCD-2) performed as part of the patients' clinical evaluations were extracted from the patients' medical records. Data from a historic normal control group ($N$ = 27) are presented next to the proportions from iMCD-1 and iMCD-2 for reference, but no statistical tests were performed (17). A panel of iMCD experts assembled for the ACCELERATE Natural History Registry reviewed clinical data and histopathology for each case, confirming each diagnosis and grading the key histopathological features. Medical record and imaging data were reviewed by the treating physician to assess the symptomatic response by MCD-OSS and tumor/lymph node response criteria (as defined in ref. 10) as well as clinical benefit response (as defined in ref. 21).

*Flow cytometry*. Samples from 3 patients (during flare and remission) and 3 age- and sex-matched healthy controls were collected and processed following the same protocol. Briefly, PBMCs were isolated by density gradient centrifugation using Ficoll-Paque PLUS (GE Healthcare). Cells were washed twice in phosphate-buffered saline (PBS) (Life Technologies), cryopreserved in freezing medium containing 20% fetal bovine serum (FBS) (Life Technologies) and 10% DMSO (Sigma-Aldrich), and maintained in liquid nitrogen for long-term storage. iMCD-1's flare sample was collected when iMCD-1's CRP was 28.5 mg/L before receiving VDT-ACE-R, which induced a partial response. The remission sample was collected 3 months after the patient received VDT-ACE-R chemotherapy and was in a complete remission on sirolimus. iMCD-2's flare sample was collected upon relapse of symptoms while on tocilizumab immediately before sirolimus monotherapy was initiated. The remission sample was collected 6 months after sirolimus monotherapy was initiated. Samples obtained from 1 month and 3 months after the initiation of sirolimus were also analyzed and demonstrated a similar trend (data not shown). iMCD-3's flare sample was collected upon relapse of symptoms while on tocilizumab immediately before sirolimus monotherapy was initiated. The remission sample was collected 6 months after sirolimus was initiated. Samples obtained from 1 month and 3 months after the initiation of sirolimus were also analyzed and demonstrated a similar trend (data not shown). For flow cytometry experiments, cryopreserved cells were thawed and rested for 3 hours in RPMI medium supplemented with 10% FBS (Gemini), 1% penicillin/streptomycin (Lonza), and 2 mM L-glutamine (Corning). Cells were then washed with PBS and stained with a viability dye (LIVE/DEAD Aqua, Thermo Fisher Scientific) for 10 minutes at room temperature, followed by 20 minutes of staining with antibodies against surface markers. Antibody clones used were as follows: anti-CD3 (UCHT1, BD Biosciences, catalog 565515), anti-CD4 (SK3, BD Biosciences, catalog 566392), anti-CD8 (RPA-T8, BD Biosciences, catalog 564805), anti-CD19 (HIB19, BioLegend, catalog 302239), anti-CD14 (MϕP9, BD Biosciences, catalog 566190), anti-CD45RA (HI100, BD Biosciences, catalog 565702), anti-CCR7 (G043H7, BioLegend, catalog 353213), anti-CD27 (O323, BioLegend, catalog 302827), anti–HLA-DR (G46-6, BD Biosciences, catalog 562844), anti-CD38 (HIT2, BD Biosciences, catalog 565069), and anti-PD1 (EH12.2H7, BioLegend, catalog 562516). After staining, cells were washed with PBS containing 1% BSA (Gemini) and 0.1% sodium azide (Thermo Fisher Scientific) and fixed with 1% paraformaldehyde (EMS). All samples were read using a FACSymphony A5 cytom-

eter (BD Biosciences) and analyzed using FlowJo software (FlowJo, LLC). Lymphocytes were identified by forward and side scatter. The lymphocyte gate was further analyzed to gate live $CD3^+CD8^+$ T cells. Nonnaive $CD8^+$ T cells were gated by excluding $CD45RA^+CCR7^+$ cells, which represent naive $CD8^+$ T cells. An unpaired 1-tailed Student's *t* test was used to compare the proportions of cell populations in iMCD flare samples versus healthy controls. A paired 1-tailed Student's *t* test was used to compare the proportions of cell populations in iMCD samples obtained during flare versus matched remission samples while on treatment with sirolimus.

*Proteomics*. The third and fifth flare samples for iMCD-1 were both collected at the onset of the third and fifth flares, respectively, when CRP levels were between 2–3 times the ULN. The remission serum and plasma samples were collected when iMCD-1's CRP was in the normal range. Serum and plasma were isolated for iMCD-1 following standard protocols, stored at –80°C, and shipped overnight on dry ice to Myriad RBM (serum) and SomaLogic, Inc. (plasma) for analysis. Proteomic quantifications were performed in accordance with previously published methods for Myriad RBM DiscoveryMAP v.3.3 (41), a multiplex immunoassay that quantifies the levels of 315 analytes, and SomaLogic SOMAscan (42), a modified DNA-aptamer approach that quantifies 1129 analytes.

*DiscoveryMAP data set*. Of the 315 proteins profiled using DiscoveryMAP, 236 were detectable across all 3 samples, 41 were detectable in at least 1 sample, and 38 were not detectable in any of the samples. The average expression of each protein with complete or some missing data was compared with the least detectable dose (LDD). All proteins detectable in at least 1 sample had an average expression that was greater than the LDD. Therefore, any missing values were replaced with the LDD for that given protein. Last, IL-6 was removed from the analyses because following siltuximab administration, its levels cannot be accurately measured by currently available immunologic-based IL-6 quantification due to interference by IL-6–neutralized siltuximab complexes (43). The $\log_2$ ratio of protein concentration in flare divided by remission was established for every protein for both flares to generate a heatmap. Proteins with an absolute $\log_2$ fold-change greater than 2 were analyzed using Enrichr, a web-based application that allows the user to upload a list of gene symbols, with a Fisher's exact test being used to compare the gene list with gene sets from a given database. KEGG 2016 was used to identify significantly enriched metabolic pathways. The Library of Integrated Network-based Cellular Signatures (LINCS) 1000 database (approximately 1300 FDA-approved drugs) was used to identify drugs that could reverse the gene expression of upregulated proteins. The Benjamini-Hochberg false discovery rate (FDR < 0.01) was used to correct for multiple hypothesis testing.

*SOMAscan data set*. To identify canonical pathways, Ingenuity Pathway Analysis (Qiagen) (44) was performed on the SOMAscan quantified proteins that demonstrated at least a 2-fold change between flare and remission (e.g., absolute value of $\log_2$ [flare/remission] ≥ 1) independently for each flare. The reference data set consisted of all 1129 proteins quantified by SOMAscan. Fisher's exact test *P* value (–log [*P* value]) measuring overlap of observed and predicted regulated gene sets were generated for each canonical pathway in accordance with previously published methods (4).

*Immunohistochemistry*. Immunohistochemistry (IHC) of formalin-fixed paraffin-embedded tissue sections was performed at the Pathology Core at the Children's Hospital of Philadelphia following standard protocols. Briefly, slides were generated at 5-μm thickness for iMCD-1, iMCD-2, and iMCD-3, 5 patients with autoimmune lymphoproliferative syndrome, and 6 patients with reactive lymph nodes excised. Epitope retrieval was done for 20 minutes with E1 retrieval solution (Leica Biosystems). IHC was performed on a Leica Bond Max automated staining system (Leica Biosystems) using the Bond Intense R staining kit (Leica Biosystems DS9263). Anti-phospho-S6 ribosomal protein (Ser235/236) (D57.2.2E, Cell Signaling Technology, catalog 4851S) was used at a 1:125 dilution and an extended incubation time of 1 hour at room temperature. Avidin Biotin Blocking was added (Vector Labs SP-2001) and a Peptide Blocking step was included (DAKO X0909). Slides were digitally scanned at ×20 magnification on an Aperio ScanScope CS-O slide scanner (Leica Biosystems) and analyzed offline using Aperio ImageScope and Image Analysis Toolkit software (color deconvolution v9 algorithm). Quantification of germinal center staining intensity and quantification of interfollicular staining intensity was performed as the percentage of pixels stained positive as well as weak, medium, or strong. Hematoxylin and eosin (H&E) staining was conducted using standard protocols at the Anatomical Pathology Division of the Pathology Clinical Service Center.

*Statistics*. Detailed information regarding statistical tests used and significance (*P* values) for each figure panel are specified in the respective figure legends. For comparisons of flow cytometry data between 2 groups where the preexperiment hypothesis being tested was that one particular group was increased compared with the other group, 1-tailed Student's *t* tests were performed. Statistical analysis of the comparison of IHC stained–area proportions between subjects and controls was performed using compositional analysis, as the different stained-intensity area proportions add up to 1 and are dependent on each other. Proportion data were converted using the centrometric log-ratio transformation. A 1-tailed nonparametric Mann-Whitney *U* test was used to compare between cases and control groups. A *P* value less than 0.05 was considered significant. All IHC compositional analysis code was written in R version 3.4.4. Proteomics data was transformed and graphed using R version 3.4.4. Flow cytometry data analyses were performed using FlowJo and GraphPad Prism. The remaining statistical analyses were performed using Microsoft Excel.

*Study approval*. All studies were approved by the University of Arkansas for Medical Sciences' or University of Pennsylvania's institutional review boards. Patients provided written informed consent prior to inclusion in the study.

## Author contributions

DCF conducted data analyses, contributed to study design, and contributed to writing the manuscript. RAL and ASJ conducted laboratory experiments, conducted data analyses, and contributed to writing the manuscript. AR, TK, MBJ, ADC, JRR, CSN, VK, FVR, and MRB contributed to study design and data interpretation. TSU, GBW, A Schwarer, MRB, FFJ, NH, KS, and ADC contributed to study design, clinical data and sample collection, and characterization of subjects. HLP, SKP, A Singh, RAL, MO, and DJA contributed to data collection and analysis. All authors reviewed and approved the final manuscript.

## Acknowledgments

We wish to thank Kathleen Sullivan and Melanie Ruffner for assistance with proteomics pathway analysis. We wish to thank Duncan

Mackay, Grant Mitchell, Daniel Rader, Joseph Baur, Matt Weitzman, Vandana Chaturvedi, and Nancy Speck for their consultations on this study. We wish to thank Dustin Shilling, Rozena Rasheed, Clarice Dard, Marjorie Raines, David Chillura, and Amy Liu for their important contributions to Castleman disease research and to this study. We wish to thank Alanna Mara PS Bezerra and Dra Denise Pasqualin for their important contributions to this study. We wish to thank the ACCELERATE Certification & Access Subcommittee, including Gordan Srkalovic, Corey Casper, Elaine Jaffe, Amy Chadburn, and Megan Lim for their review of each case and histopathological scores. We wish to thank the Anatomical Pathology Division of the Pathology Clinical Service Center and the Pathology Core at the Children's Hospital of Philadelphia, in particular, Daniel Martinez, for technical assistance. This work was funded by the Castleman's Awareness & Research Effort (to VPK and DCF), Penn Center for Precision Medicine (to DCF), University of Pennsylvania University Research Foundation (to DCF), Intramural NIH funding (ZIA BC 011700 to TSU), and National Heart Lung and Blood Institute of the National Institutes of Health (R01-HL141408 to DCF).

Address correspondence to: David C. Fajgenbaum, University of Pennsylvania, 3620 Hamilton Walk, Anatomy-Chemistry, Suite 214, Philadelphia, Pennsylvania 19104, USA. Phone: 215.614.0936; Email: davidfa@pennmedicine.upenn.edu.

1. Munshi N, Mehra M, van de Velde H, Desai A, Potluri R, Vermeulen J. Use of a claims database to characterize and estimate the incidence rate for Castleman disease. *Leuk Lymphoma*. 2015;56(5):1252–1260.
2. Soulier J, et al. Kaposi's sarcoma-associated herpesvirus-like DNA sequences in multicentric Castleman's disease. *Blood*. 1995;86(4):1276–1280.
3. Liu AY, et al. Idiopathic multicentric Castleman's disease: a systematic literature review. *Lancet Haematol*. 2016;3(4):e163–e175.
4. Fajgenbaum DC, et al. International, evidence-based consensus diagnostic criteria for HHV-8-negative/idiopathic multicentric Castleman disease. *Blood*. 2017;129(12):1646–1657.
5. Kawabata H, et al. Castleman-Kojima Disease (TAFRO Syndrome): a novel systemic inflammatory disease characterized by a constellation of symptoms, namely, thrombocytopenia, ascites (anasarca), microcytic anemia, myelofibrosis, renal dysfunction, and organomegaly: a status report and summary of Fukushima (6 June, 2012) and Nagoya Meetings (22 September, 2012). *J Clin Exp Hematop*. 2013;53(1):57–61.
6. Dispenzieri A, et al. The clinical spectrum of Castleman's disease. *Am J Hematol*. 2012;87(11):997–1002.
7. Beck JT, et al. Brief report: alleviation of systemic manifestations of Castleman's disease by monoclonal anti-interleukin-6 antibody. *N Engl J Med*. 1994;330(9):602–605.
8. Yoshizaki K, et al. Pathogenic significance of interleukin-6 (IL-6/BSF-2) in Castleman's disease. *Blood*. 1989;74(4):1360–1367.
9. Nishimoto N, et al. Humanized anti-interleukin-6 receptor antibody treatment of multicentric Castleman disease. *Blood*. 2005;106(8):2627–2632.
10. van Rhee F, et al. Siltuximab for multicentric Castleman's disease: a randomised, double-blind, placebo-controlled trial. *Lancet Oncol*. 2014;15(9):966–974.
11. van Rhee F, et al. International, evidence-based consensus treatment guidelines for idiopathic multicentric Castleman disease. *Blood*. 2018;132(20):2115–2124.
12. Iwaki N, et al. Elevated serum interferon γ-induced protein 10 kDa is associated with TAFRO syndrome. *Sci Rep*. 2017;7:42316.
13. Saxton RA, Sabatini DM. mTOR signaling in growth, metabolism, and disease. *Cell*. 2017;168(6):960–976.
14. Völkl S, et al. Hyperactive mTOR pathway promotes lymphoproliferation and abnormal differentiation in autoimmune lymphoproliferative syndrome. *Blood*. 2016;128(2):227–238.
15. Fruman DA, Chiu H, Hopkins BD, Bagrodia S, Cantley LC, Abraham RT. The PI3K pathway in human disease. *Cell*. 2017;170(4):605–635.
16. Fajgenbaum DC, Fajgenbaum D, Rosenbach M, van Rhee F, Nasir A, Reutter J. Eruptive cherry hemangiomatosis associated with multicentric Castleman disease: a case report and diagnostic clue. *JAMA Dermatol*. 2013;149(2):204–208.
17. Battaglia A, et al. Lymphocyte populations in human lymph nodes. Alterations in CD4+ CD25+ T regulatory cell phenotype and T-cell receptor Vbeta repertoire. *Immunology*. 2003;110(3):304–312.
18. Magnuson B, Ekim B, Fingar DC. Regulation and function of ribosomal protein S6 kinase (S6K) within mTOR signalling networks. *Biochem J*. 2012;441(1):1–21.
19. Lim MS, et al. Pathological findings in human autoimmune lymphoproliferative syndrome. *Am J Pathol*. 1998;153(5):1541–1550.
20. Teachey DT, et al. Treatment with sirolimus results in complete responses in patients with autoimmune lymphoproliferative syndrome. *Br J Haematol*. 2009;145(1):101–106.
21. van Rhee F, et al. Siltuximab, a novel anti-interleukin-6 monoclonal antibody, for Castleman's disease. *J Clin Oncol*. 2010;28(23):3701–3708.
22. Cheson BD, et al. Revised response criteria for malignant lymphoma. *J Clin Oncol*. 2007;25(5):579–586.
23. Zhao DQ, Li SW, Sun QQ. Sirolimus-based immunosuppressive regimens in renal transplantation: a systemic review. *Transplant Proc*. 2016;48(1):3–9.
24. McCormack FX, et al. Efficacy and safety of sirolimus in lymphangioleiomyomatosis. *N Engl J Med*. 2011;364(17):1595–1606.
25. Guba M, et al. Rapamycin inhibits primary and metastatic tumor growth by antiangiogenesis: involvement of vascular endothelial growth factor. *Nat Med*. 2002;8(2):128–135.
26. Hudson CC, et al. Regulation of hypoxia-inducible factor 1alpha expression and function by the mammalian target of rapamycin. *Mol Cell Biol*. 2002;22(20):7004–7014.
27. Kim DD, et al. Rapamycin inhibits VEGF-induced microvascular hyperpermeability in vivo. *Microcirculation*. 2010;17(2):128–136.
28. Medici D, Olsen BR. Rapamycin inhibits proliferation of hemangioma endothelial cells by reducing HIF-1-dependent expression of VEGF. *PLoS ONE*. 2012;7(8):e42913.
29. Wang W, et al. Antitumoral activity of rapamycin mediated through inhibition of HIF-1alpha and VEGF in hepatocellular carcinoma. *Dig Dis Sci*. 2009;54(10):2128–2136.
30. Ghosh P, Buchholz MA, Yano S, Taub D, Longo DL. Effect of rapamycin on the cyclosporin A-resistant CD28-mediated costimulatory pathway. *Blood*. 2002;99(12):4517–4524.
31. Perl A. mTOR activation is a biomarker and a central pathway to autoimmune disorders, cancer, obesity, and aging. *Ann N Y Acad Sci*. 2015;1346(1):33–44.
32. Salmond RJ, Brownlie RJ, Meyuhas O, Zamoyska R. Mechanistic target of rapamycin complex 1/S6 kinase 1 signals influence T Cell activation independently of ribosomal protein S6 phosphorylation. *J Immunol*. 2015;195(10):4615–4622.
33. Sehgal SN, Bansbach CC. Rapamycin: in vitro profile of a new immunosuppressive macrolide. *Ann N Y Acad Sci*. 1993;685:58–67.
34. Xiong M, Elson G, Legarda D, Leibovich SJ. Production of vascular endothelial growth factor by murine macrophages: regulation by hypoxia, lactate, and the inducible nitric oxide synthase pathway. *Am J Pathol*. 1998;153(2):587–598.
35. Lai ZW, et al. Sirolimus in patients with clinically active systemic lupus erythematosus resistant to, or intolerant of, conventional medications: a single-arm, open-label, phase 1/2 trial. *Lancet*. 2018;391(10126):1186–1196.
36. Pierson SK, et al. Plasma proteomics identifies a 'chemokine storm' in idiopathic multicentric Castleman disease. *Am J Hematol*. 2018;93(7):902–912.
37. Beran O, Holub M, Spála J, Kalanin J, Stanková M. Cd38 expression on Cd8+ T cells in human immunodeficiency virus 1-positive adults treated with HAART. *Acta Virol*. 2003;47(2):121–124.
38. Pavón EJ, et al. Increased CD38 expression in T cells and circulating anti-CD38 IgG autoantibodies differentially correlate with distinct cytokine profiles and disease activity in systemic lupus erythematosus patients. *Cytokine*. 2013;62(2):232–243.
39. Nagelkerke SQ, Kuijpers TW. Immunomodulation by IVIg and the role of Fc-Gamma receptors: classic mechanisms of action after all? *Front Immunol*. 2014;5:674.
40. Nabel CS, et al. Virome capture sequencing does

not identify active viral infection in unicentric and idiopathic multicentric Castleman disease. *PLoS ONE*. 2019;14(6):e0218660.
41. Walcott BP, Patel AP, Stapleton CJ, Trivedi RA, Young AMH, Ogilvy CS. Multiplexed protein profiling after aneurysmal subarachnoid hemorrhage: characterization of differential expression patterns in cerebral vasospasm. *J Clin Neurosci*. 2014;21(12):2135–2139.
42. Gold L, et al. Aptamer-based multiplexed proteomic technology for biomarker discovery. *PLoS ONE*. 2010;5(12):e15004.
43. Casper C, et al. Analysis of inflammatory and anemia-related biomarkers in a randomized, double-blind, placebo-controlled study of siltuximab (anti-IL6 monoclonal antibody) in patients with multicentric Castleman disease. *Clin Cancer Res*. 2015;21(19):4294–4304.
44. Krämer A, Green J, Pollard J, Tugendreich S. Causal analysis approaches in ingenuity pathway analysis. *Bioinformatics*. 2014;30(4):523–530.